MITIGATION OF BACKGROUND EMI, MECHANICAL AND ACOUSTIC EFFECTS FROM THE GAMBLE II PULSED POWER GENERATOR [*]

D. P. Murphy[ξ], B. V. Weber, R. J. Allen and G. Cooperstein
Naval Research Laboratory, Plasma Physics Division, Washington DC 20375
F. C. Young
Jaycor/Titan, McLean VA 22102

Abstract

The Gamble II accelerator can be used with several diode configurations to provide a diverse x-ray spectrum to different test packages. For example, in Bremsstrahlung mode, the Gamble II accelerator typically injects a 600-700 kA, 1.2-1.4 MV electron beam into a tantalum x-ray converter to produce x-ray Bremsstrahlung. However, along with the radiation flux, the test package may be subjected to unwanted electromagnetic interference (EMI) or mechanical and acoustic effects that can confuse the test results. Most of the EMI and mechanical effects are generated in the power conditioning sections of Gamble II. We have undertaken a series of measurements using calibrated RF antennas and accelerometers to find the sources of EMI and mechanical effects. These measurements will be used to design upgrades to the pulsed power system that will minimize any detrimental impact on the test packages.

I. DESCRIPTION OF THE EMI PROBLEM

Gamble II can produce a 1-2 MV, 0.5-1 MA pulse with about 100-ns pulse duration. The generator is (nominally) a coaxial transmission line, so the electric and magnetic fields outside the generator should be zero. In reality, there are several locations where fields can propagate outside the generator and these are measurable with appropriate antennae. The timing of the signals helps to identify the source of the radiation, as Gamble II works by sequentially firing several switches. The setup is shown below in the cross section line drawing and the color drawing (Fig. 1). The first switches fired are located in the Marx bank, next the water switch closes and finally the oil output switch fires. The test object is located in front of the machine, so EMI measurements should be made there. Measurements at other locations help to identify the noise sources for mitigation purposes.

The device holder for radiation effects testing is shown in front of Gamble II (Fig. 2). The holder is mounted on a vibration-isolation table. X-rays from Gamble II pass through a vacuum isolation section that reduces acoustic shock to the device under test (DUT). The endplates of
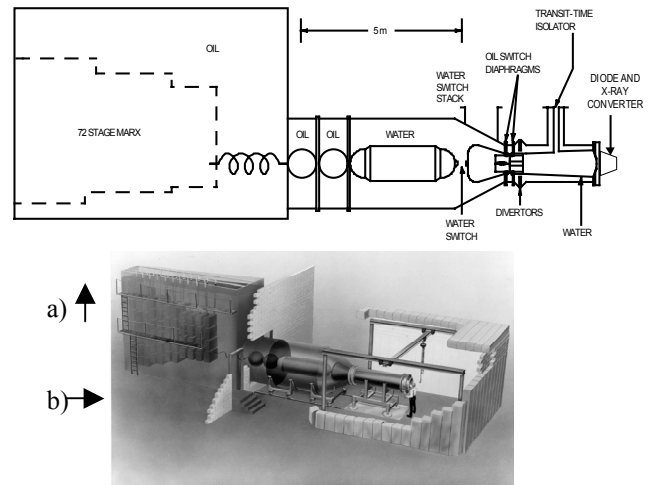

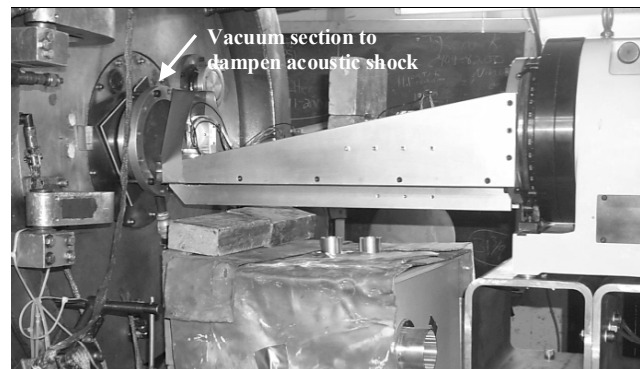**Figure 1.** a)Line drawing cross section of Gamble II b)color drawing of Gamble II.

Figure 2. Radiation Effects Test Stand shown in front of Gamble II.

the vacuum section shown here are melamine (plastic).

II. EMI SENSORS (ANTENNAE AND B-DOTS)

We have selected the EG&G models ACD-3 and ACD-4 D-dot probes to accurately measure the EMI emitted by Gamble II. A photograph showing the ACD-3 probe (monopole) is in Figure 3 and the ACD-4 probe (dipole) is shown in Figure 4. There are many different types of antennas that can be used to measure RF

[ξ] email: donald.murphy@nrl.navy.mil

891

Report Documentation Page

Public reporting burden for the collection of information is estimated to average 1 hour per response, including the time for reviewing instructions, searching existing data sources, gathering and maintaining the data needed, and completing and reviewing the collection of information. Send comments regarding this burden estimate or any other aspect of this collection of information, including suggestions for reducing this burden, to Washington Headquarters Services, Directorate for Information Operations and Reports, 1215 Jefferson Davis Highway, Suite 1204, Arlington VA 22202-4302. Respondents should be aware that notwithstanding any other provision of law, no person shall be subject to a penalty for failing to comply with a collection of information if it does not display a currently valid OMB control number.

1. REPORT DATE **JUN 2003**	2. REPORT TYPE **N/A**	3. DATES COVERED **-**	
4. TITLE AND SUBTITLE **Mitigation Of Background Emi, Mechanical And Acoustic Effects From The Gamble Ii Pulsed Power Generator**		5a. CONTRACT NUMBER	
		5b. GRANT NUMBER	
		5c. PROGRAM ELEMENT NUMBER	
6. AUTHOR(S)		5d. PROJECT NUMBER	
		5e. TASK NUMBER	
		5f. WORK UNIT NUMBER	
7. PERFORMING ORGANIZATION NAME(S) AND ADDRESS(ES) **Naval Research Laboratory, Plasma Physics Division, Washington DC 20375**		8. PERFORMING ORGANIZATION REPORT NUMBER	
9. SPONSORING/MONITORING AGENCY NAME(S) AND ADDRESS(ES)		10. SPONSOR/MONITOR'S ACRONYM(S)	
		11. SPONSOR/MONITOR'S REPORT NUMBER(S)	

12. DISTRIBUTION/AVAILABILITY STATEMENT
Approved for public release, distribution unlimited

13. SUPPLEMENTARY NOTES
See also ADM002371. 2013 IEEE Pulsed Power Conference, Digest of Technical Papers 1976-2013, and Abstracts of the 2013 IEEE International Conference on Plasma Science. IEEE International Pulsed Power Conference (19th). Held in San Francisco, CA on 16-21 June 2013. U.S. Government or Federal Purpose Rights License

14. ABSTRACT
The Gamble II accelerator can be used with several diode configurations to provide a diverse x-ray spectrum to different test packages. For example, in Bremsstrahlung mode, the Gamble II accelerator typically injects a 600- 700 kA, 1.2-1.4 MV electron beam into a tantalum x-ray converter to produce x-ray Bremsstrahlung. However, along with the radiation flux, the test package may be subjected to unwanted electromagnetic interference (EMI) or mechanical and acoustic effects that can confuse the test results. Most of the EMI and mechanical effects are generated in the power conditioning sections of Gamble II. We have undertaken a series of measurements using calibrated RF antennas and accelerometers to find the sources of EMI and mechanical effects. These measurements will be used to design upgrades to the pulsed power system that will minimize any detrimental impact on the test packages.

15. SUBJECT TERMS

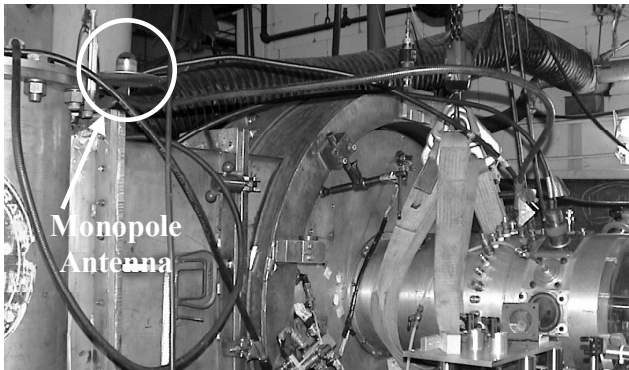| 16. SECURITY CLASSIFICATION OF:			17. LIMITATION OF ABSTRACT **SAR**	18. NUMBER OF PAGES **4**	19a. NAME OF RESPONSIBLE PERSON
a. REPORT **unclassified**	b. ABSTRACT **unclassified**	c. THIS PAGE **unclassified**			

Figure 3. ACD-3 monopole antenna mounted on top of the diffusion pump near the front of Gamble II.

radiation fields, but D-dots and B-dots are normally used in this type of application because of their flat response over a wide range of frequencies. The ACD-3 and ACD-4 probes have virtually flat frequency responses from DC to >1GHz (3dB point). This upper frequency limit is well matched to that of our digitizers (500MHz analog bandwidth). There are B-dot probes that also have a wide frequency response, but the ACD-4 dipole probe has the highest sensitivity at this bandwidth of all commercially available probes known to us. The ACD-3 probe is a monopole version of the ACD-4 probe, allowing it to be placed directly onto a ground plane. The ACD-3 probe has the same bandwidth as the ACD-4 probe, but half the sensitivity and size.

The voltage output of both D-dot and B-dot probes is often specified in terms of their equivalent area, A_{eq}, and load impedance, R. In general, A_{eq} increases with the physical size of the probe, but bandwidth decreases with size. The impedance of the signal cable is usually chosen for R to avoid reflections from the end of the cable. The output voltage, V_0, of the ACD probe is given by:

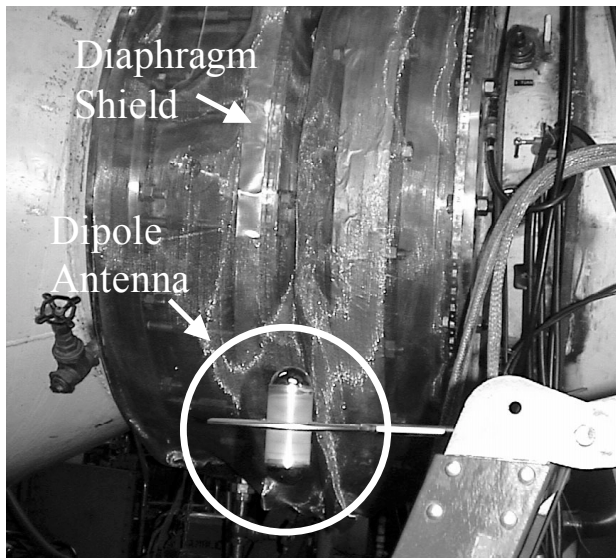$$V_o = RA_{eq} \frac{dD}{dt} \cos \theta \qquad (1)$$

Figure 4. ACD-4 dipole antenna mounted near the oil switch on Gamble II.

where $\frac{dD}{dt}$ [in units of C/m^2/s] (called "D-dot") is the time derivative of electric flux density [C/m^2]. A_{eq} is given as 0.01 m^2 for both ACD-3 and ACD-4 probes, but R is 50 Ω for the ACD-3 probe and 100 Ω for the ACD-4 probe. Since we are using 50 Ω signal cable, we are using the EG&G model DMB-3E balun to transform the 100 Ω input into a 50 Ω output. This balun gives an attenuation of 6dB, so both the ACD-3 and ACD-4 probes give the same output voltage for a given field in our configuration.

The orientation of probe with respect to the D vector is represented by the $\cos \theta$ term. For far field measurements D will be normal to a line from the source to the probe. Also, the magnetic field is related to the electric field by E/H=377 Ω, where D=ε$_0E$, E is the electric field intensity in V/m and ε$_0$ is the permittivity of free space (8.85x10^{-12} F/m). However, in the near field case (as our measurements likely are) three orthogonal measurements are required to determine the total E vector, and there is no simple relationship between E and H.

To determine the electric field, E, it is necessary to integrate V_0. This can be done either numerically or with a hardware integrator. We numerically integrate because of the added complexity that the hardware integrator involves. The frequency response of the hardware integrator often requires numerical correction for droop. The main problems with numerical integration are baseline correction and baseline drift, although both of these can be corrected to some extent.

A set of three B-dot sensors with orthogonal orientations was made in-house. The probes are mounted using threaded N connectors in a block of acrylic as shown in Figure 5. The block is clamped in position and all three B-field components can be measured simultaneously. So far, this probe set was used to make measurements on top of the transit-time isolator and on top of the water switch stack (see Fig. 1).
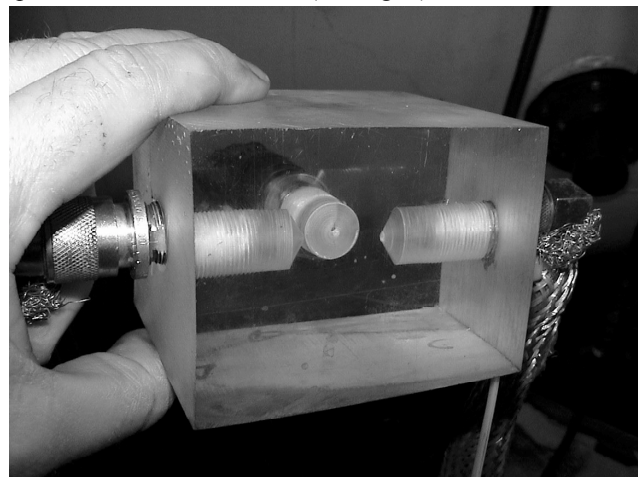

Figure 5. Three B-dot sensors with orthogonal orientations were used to probe electromagnetic interference (EMI).

III. EMI CHARACTERIZATION

Sample data from short-circuit shot 8369 are shown in Figure 6. The antennae signals are plotted in units of V/m/s (the calibration is $2.26x10^{11}$ V/m/s per volt recorded on the digitizer). The timing of the various switches in Gamble II is also indicated in the figure. The marx switches fire earlier than the time window of the antenna signals and probably contribute negligible noise. The water switch fires at t = -0.26 µs and a small signal increase is evident on the antennae. The oil switch fires at t = -0.04 µs, slightly later than the start of the large antennae signals. The monitor used to determine the oil switch firing time (transformer input current) is located downstream in water. There is some transit time (9 ns/foot) that delays this signal relative to the actual switch closure time, so we conclude that the large EMI signal is caused by the oil switch firing. The power pulse reaches the front end of the machine at t = +0.05 µs, significantly later than the onset of the noise signals.

An important feature of the data in Figure 6 is the time delay between the two antenna signals. The dipole, located near the oil switch, begins about 8 ns earlier than the monopole, located near the front end. This is about equal to the time of flight for EM radiation to travel through air (1 ns/foot) from the oil switch to the front of the machine, evidence that the EMI emanates from the vicinity of the oil switch.

The ACD signal integrity was tested by covering the dipole antenna probe with copper screen. The resulting signal on a Gamble II shot is essentially zero compared with data from a comparable (Both shots had diode loads.). This test demonstrated that the pickup on the cables was negligible compared with the antenna signal.

The peak-peak electric field variation determined by numerical integration of the D-dot signals is as high as 25 kV/m on some shots. However, we suspect that the low frequency components of the electric field are dominated by errors associated with numerical integration, basically
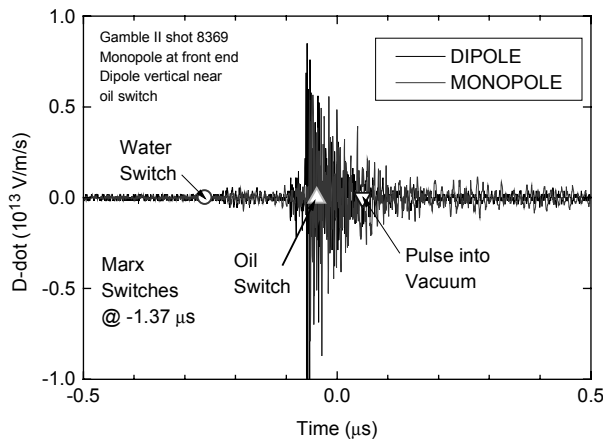

Figure 6. D-dot data from shot 8369.

amplifying low frequency noise by a factor of 1/ω. In future experiments, we will try passive integration so the E(t) signal is recorded directly on the digitizer. The

numerical integration technique introduced so much uncertainty that an alternative analysis is used in this report to compare results from different experiments.

One way to process the data for simplified comparisons is to compute an RMS waveform,

$$V_{rms} = \left[\frac{1}{t_2 - t_1} \int_{t_1}^{t_2} V^2 dt \right]^{1/2} \qquad (2)$$

Here, t_1 is the first time point in the waveform and t_2 is the last time. An example of the RMS waveform for the dipole signal is shown in Figure 7. This smooth waveform will be used to compare different mitigation techniques in the next section.
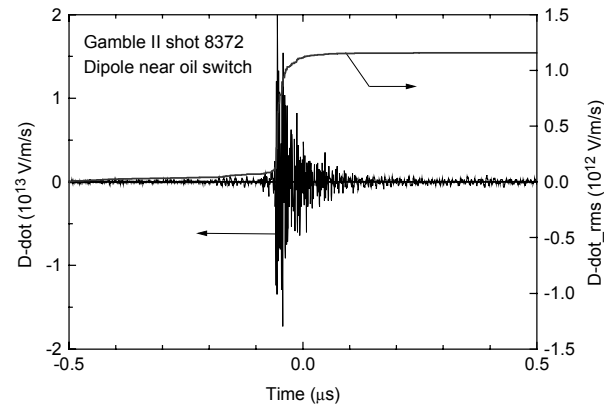

Figure 7. Raw D-dot and RMS D-dot ACD-4 signals for shot 8372.

IV. EMI MITIGATION

The oil switch is located between two water-filled sections as shown in Figure 1. Polyurethane diaphragms separate the oil from water. The electrical connections on the outer conductor are made by a large number of bolts through holes in the diaphragms. Since this electrical path is not completely symmetric, it could be a source of EM radiation. The diaphragms were covered with brass sheet and clamped to the flanges on either side using a long hose clamp. This make a continuous connection over the diaphragms. The dipole signals both showed a factor-of-two reduction in the RMS signal as shown in Figure 8, comparing "baseline" waveforms with "shield diaphragms" waveforms. (All shots had diode loads.) Another asymmetry exists where the oil switch housing seals against the downstream diaphragm. There is a gap of about 1 cm between the housing and the flange, spanned by the insulator, so the outer conductor current is conducted through long rods between the two flanges. This was improved using a helical wire gasket as a current contact to connect the housing to the flange. The resulting RMS signal level decreased by another factor of 2. The dipole data Figure 8 includes the RMS waveform for the shot with screen over the antenna, illustrating the effective baseline RMS value from the bit noise on the

893

signal. These shielding changes reduced the EMI by about one order of magnitude, but did not eliminate it. A copper mesh cover was constructed with fingerstock current contacts to span the oil switch and diverter switch sections in an attempt to further improve the shielding. This shield is shown in Figure 4. The antenna signals did not appear to decrease using this additional shield, probably an indication that the residual signal emanates from another location.
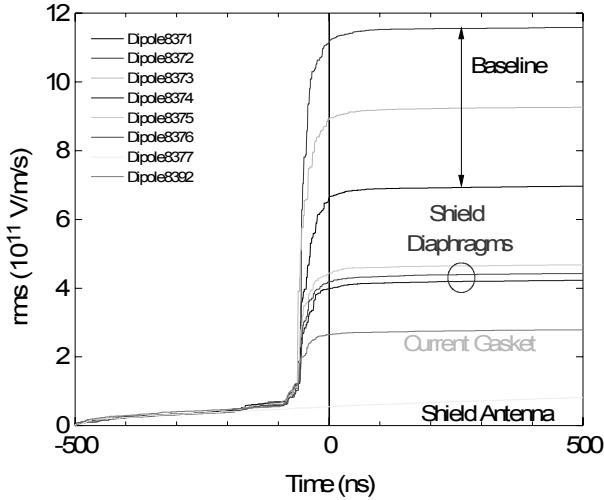

Figure 8. RMS Dipole data with various shielding strategies.

A later sequence of shots (using dielectric end plates), and only 1/7th of the normal Gamble II current, shows the potential for large EMI signals produced from the front end (diode region), as shown in Figure 9. Two of the seven consecutive shots have RMS monopole signals 3.5 times larger than the other five shots. The larger signals depart from the others at about t = 100 ns, the time the power reaches the front end of the machine. These two shots were different from the other five in that the electron beam was injected through a thin anode foil into an evacuated cylindrical chamber. The other shots injected electrons into the same chamber but with 1 torr
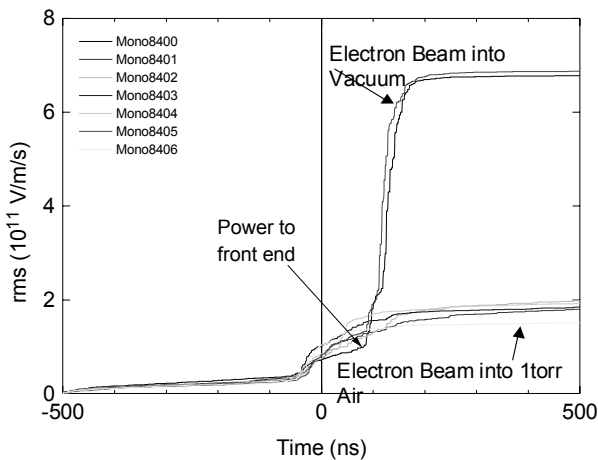

Figure 9. RMS Monopole data with electron beam into target chamber at different air pressures.

air. The vacuum shots produced EM radiation and the radiation could propagate through the dielectric end plate into the room, where the monopole antenna at the front end picked it up. When the beam is injected into gas, current and charge neutralization greatly reduce the chance for any radiation. In fact, the dipole antenna near the oil switch does not show an increased signal at that time for this shot sequence.
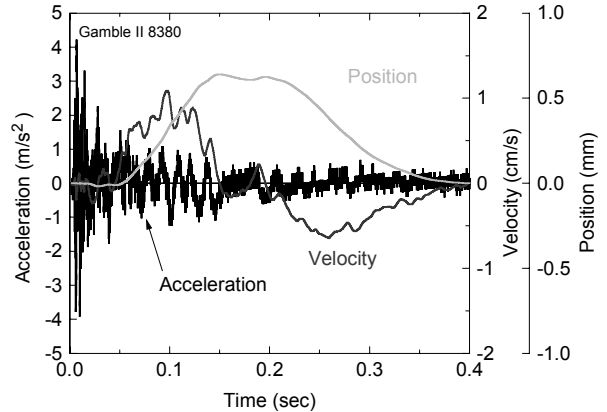

Figure 10. Measured PZT acceleration with the calculated velocity and position of the concrete floor after a Gamble II shot.

V. GROUND SHOCK MEASUREMENTS

Approximately $2x10^5$ joules of stored energy are released on each Gamble II shot. Some of the energy is mechanically coupled to the floor. This can affect the device under test (DUT). A piezo-electric transducer (PZT) was glued to the concrete floor in front of Gamble II during some shots to measure the acceleration to which the isolation table is subjected. The measured acceleration is used to calculate the velocity and vertical motion of the floor after the shot (see Figure 10). Within 0.25 sec the reinforced concrete floor in front of Gamble II flexes by as much as 0.5 mm. This is sufficient to disturb sensitive measurements on the DUT if the isolation table does not adequately damp the motion.

VI.   FUTURE PLANS

The antennae and B-dot array can be used in the future for evaluating other mitigation efforts on Gamble II. The front of the vacuum section will be metal instead of melamine. Other openings in the outer conductor should be evaluated to find the greatest remaining sources of EMI. More sensitive PZTs will be mounted on both the floor and on the isolation table for future shots. A dedicated series of shots in the bremsstrahlung configuration with the test fixture in front of Gamble II is planned. Then, we can diagnose EMI and shock/acoustic noise and decide if further mitigation is necessary and how best to accomplish it.